# Systematic effects in the $HfF^+$-ion experiment to search for the electron electric dipole moment

A. N. Petrov*

*National Research Centre "Kurchatov Institute" B.P., Konstantinov Petersburg Nuclear Physics Institute, Gatchina, Leningrad District 188300, Russia*

*and Saint Petersburg State University, 7/9 Universitetskaya nab., St. Petersburg 199034, Russia*

(Received 17 September 2017; published 11 May 2018)

The energy splittings for $J = 1$, $F = 3/2$, $|m_F| = 3/2$ hyperfine levels of the $^3\Delta_1$ electronic state of $^{180}Hf^{19}F^+$ ion are calculated as functions of the external variable electric and magnetic fields within two approaches. In the first one, the transition to the rotating frame is performed, whereas in the second approach, the quantization of rotating electromagnetic field is performed. Calculations are required for understanding possible systematic errors in the experiment to search for the electron electric dipole moment ($e$EDM) with the $^{180}Hf^{19}F^+$ ion.

DOI: 10.1103/PhysRevA.97.052504

## I. INTRODUCTION

The search for the electron electric dipole moment ($e$EDM) $d_e$ is one of the most sensitive tests to date for extensions of the standard model [1,2]. Very recently, Cairncross *et al.* obtained the limit $|d_e| < 1.3 \times 10^{-28}$ $e$ cm (90% confidence) using trapped $^{180}Hf^{19}F^+$ ions [3]. The result is in agreement with the best limit of $|d_e| < 0.9 \times 10^{-28}$ $e$ cm (90% confidence) obtained in Ref. [4] with a molecular beam of the thorium monoxide (ThO) molecules.

The measurements were performed on the ground rotational, $J$=1, level in the metastable electronic $H^3\Delta_1$ state of $^{180}Hf^{19}F^+$ using the *rotating* electric and magnetic fields. Consistent with zero $e$EDM-sensitive frequency [see Eq. (3) below],

$$f^{\mathcal{BD}}/h = 0.10 \pm 0.87_{\rm stat} \pm 0.20_{\rm syst}\ \text{mHz} \tag{1}$$

was measured in the experiment. The second-generation $e$EDM experiment is projected to provide an order-of-magnitude-higher $e$EDM sensitivity than the current limit [3]. It is rather clear though that the increase in statistical sensitivity is only reasonable up to the level where systematic effects start prevailing. Thus the accurate evaluation of systematic effects becomes more important with the increase in statistical sensitivity. The main systematic effect in the experiment for the $e$EDM search with $^{180}Hf^{19}F^+$ ions comes from doublet population contamination [population of lower (upper) Stark doublet when only the upper (lower) one should be populated]. The extent of the contamination is estimated from the difference between measured and predicted (calculated) values of $f^{\mathcal{D}}$ [see Eq. (3) below] [3]. Thus, an important part of the analysis of the systematic effects reduces to a theoretical study of $f^{\mathcal{D}}$ (and other) frequencies as functions of electric and magnetic fields. One of the goals of the present work is to take into account the nonadiabatic interaction of $H^3\Delta_1$ with other electronic states, which goes beyond the theoretical study of systematic effects presented in Ref. [3]. We found that accounting for the above contribution leads to agreement between the measured and calculated values of $f^{\mathcal{D}}$.

One of the most important properties determining the prospects of molecules with regards to the search for $e$EDM is the effective electric field $E_{\rm eff}$, which can be obtained only in the precise calculations of the electronic structure. The values $E_{\rm eff} = 24$ GV/cm [5,6], 22.5 GV/cm [7], and 22.7 GV/cm [8] have been obtained. However, the $e$EDM-sensitive frequency

$$f^{\mathcal{BD}} = 2 d_e E_{\rm eff} P \tag{2}$$

is proportional to both $E_{\rm eff}$ and the degree of polarization of molecule $P$, which approach unity at large electric and magnetic fields. Study of the latter as a function of electric and magnetic fields is the second goal of the paper. The same factor is for the scalar-pseudoscalar nucleus-electron neutral current interaction.

## II. ENERGY LEVELS OF $^{180}Hf^{19}F^+$

The $e$EDM-sensitive levels of $^{180}Hf^{19}F^+$ are described in detail in Refs. [3,9,10]. In brief, the $^{180}$Hf isotope is spinless, whereas the $^{19}$F isotope has a nonzero nuclear spin $I$=1/2, which gives rise to hyperfine energy splitting between levels with total momentum $F = 3/2$ and $F = 1/2$, $\mathbf{F} = \mathbf{J} + \mathbf{I}$. In the absence of external fields, each hyperfine level has two parity eigenstates known as the $\Omega$ doublet. In the external rotating electric field, the $F = 3/2$ state splits to four Stark doublets levels. Two of them with projection of the total momentum on the rotating field $m_F = \pm 3/2$ are of interest for the $e$EDM search experiment. The rotating magnetic field which is parallel or antiparallel to the rotating electric field further splits each Stark doublet to a pair of Zeeman sublevels. $m_F = \pm 3/2$ sublevels are degenerate, in the absence of rotation, at zero magnetic field. However, the rotation connects the sublevels and turns the degeneracy to a splitting at the avoided crossing between the $m_F = +3/2$ and $m_F = -3/2$ sublevels (see Fig. 1).

The energy splitting $f$ between the sublevels is measured in the experiment. The measurement of $f$ is repeated under different conditions, which can be characterized by three binary switch parameters $\tilde{\mathcal{B}}$, $\tilde{\mathcal{D}}$, $\tilde{\mathcal{R}}$ being switched from

*alexsandernp@gmail.com; http://www.qchem.pnpi.spb.ru

 

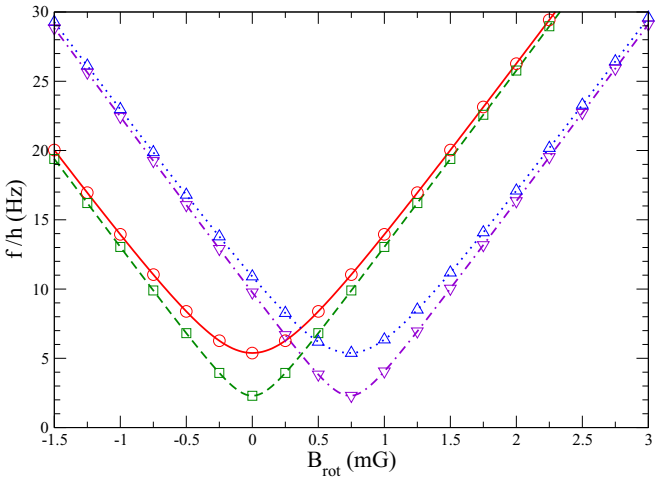


FIG. 1. Calculated energy splittings for the $H^3\Delta_1$ ($J=1, F=3/2$, $|m_F|=3/2$) Stark pairs as functions of $\mathcal{B}_{\rm rot}$. $\mathcal{E}_{\rm rot}=24$ V/cm, $\omega_{\rm rot}/2\pi=250$ kHz, $\tilde{\mathcal{R}}=+1$ in the calculations. Lines are calculated within approach I. The solid (red) line corresponds to the lower ($\tilde{\mathcal{D}}=+1$) Stark pair, $\mathcal{E}_z=0$; the dashed (green) line corresponds to the upper ($\tilde{\mathcal{D}}=-1$) Stark pair, $\mathcal{E}_z=0$; the dotted (blue) line corresponds to the lower Stark pair, $\mathcal{E}_z=0.3$ mV/cm; and the dot-dashed (purple) line corresponds to the upper Stark pair, $\mathcal{E}_z=0.3$ mV/cm. Figures are calculated within approach (II) with $N=3$. Circles (red) correspond to the lower Stark pair, $\mathcal{E}_z=0$; squares (green) correspond to the upper Stark pair, $\mathcal{E}_z=0$; up-triangles (blue) correspond to the lower Stark pair, $\mathcal{E}_z=0.3$ mV/cm; and down-triangles (purple) correspond to the upper Stark pair, $\mathcal{E}_z=0.3$ mV/cm.

$+1$ to $-1$. $\tilde{\mathcal{B}}=+1(-1)$ means that rotating magnetic field $\mathbf{B}_{\rm rot}$ is parallel (antiparallel) to rotating electric field $\mathbf{E}_{\rm rot}$, $\tilde{\mathcal{D}}=+1(-1)$ means that the measurement was performed for the lower (upper) Stark level, and $\tilde{\mathcal{R}}$ defines the direction for the rotation of the fields. An $e$EDM signal manifests as the main contribution to the $f^{\mathcal{BD}}$ channel according to Eq. (2). Here, notation $f^{S_1,S_2,\cdots}$ denotes a component which is odd under the switches $S_1, S_2, \ldots$. The notations are close to those in Refs. [11,12]. $f^{S_1,S_2,\cdots}$ can be calculated by the formula

$$f^{S_1,S_2,\cdots}(|\mathbf{B}_{\rm rot}|)=\frac{1}{8}\sum_{\tilde{\mathcal{B}},\tilde{\mathcal{D}},\tilde{\mathcal{R}}} S_1S_2\ldots f(\mathcal{B}_{\rm rot},\tilde{\mathcal{D}},\tilde{\mathcal{R}}), \qquad (3)$$

where $\mathcal{B}_{\rm rot}=\tilde{\mathcal{B}}|\mathbf{B}_{\rm rot}|=\tilde{\mathcal{B}}|\mathcal{B}_{\rm rot}|$, and $S_1, S_2, \ldots$ is a subset of the $\tilde{\mathcal{B}}$, $\tilde{\mathcal{D}}$, $\tilde{\mathcal{R}}$ parameters. For simplicity, only the dependence of $f$ on the $\mathcal{B}_{\rm rot},\tilde{\mathcal{D}},\tilde{\mathcal{R}}$ parameters is explicitly specified in Eq. (3).

Equation (2) can be understood from a simple consideration. At large fields (for a completely polarized $^{180}$Hf$^{19}$F$^+$), each of four Zeeman sublevels has a unique set of $\Omega=\pm1$, $m_F=\pm3/2$ quantum numbers, where $\Omega$ is the projection of the molecule angular momentum on the internuclear axis $\hat{n}$. Two sublevels within a Stark doublet are connected by time reversal $m_F\to -m_F$, $\Omega\to-\Omega$ and therefore have opposite signs for both $m_F$ and $\Omega$ quantum numbers. Note that $\tilde{\mathcal{D}}=\mathrm{sgn}(\Omega m_F)$. States with opposite projections of $\Omega$ have opposite projections of $\mathbf{d}_{\rm e}$ as well. Since $\mathbf{E}_{\rm eff}$ points along the internuclear axis $\hat{n}$, states with opposite projections of $\Omega$ have opposite $e$EDM energy shifts $d_eE_{\rm eff}\Omega$. In turn, the Zeeman shift is determined by $\mathrm{sgn}(m_F\tilde{\mathcal{B}})$. The Zeeman splitting is much larger than the $e$EDM one and manifests as a dominant *positive* (independently of magnetic field direction $\tilde{\mathcal{B}}$) contribution to the $f(\mathcal{B}_{\rm rot},\tilde{\mathcal{D}},\tilde{\mathcal{R}})$. The much smaller $e$EDM contribution to the splitting changes sign when the measurement is performed in the another Stark doublet [$\mathrm{sgn}(\Omega m_F)$ is changed] or when the magnetic field is reversed [$\mathrm{sgn}(m_F\tilde{\mathcal{B}})$ is changed]. Thus, the $e$EDM contribution is odd under both switches $\tilde{\mathcal{B}}$ and $\tilde{\mathcal{D}}$. For a not completely polarized $^{180}$Hf$^{19}$F$^+$, the factor $P$ has to be introduced. Note that the $e$EDM Stark shift is not related with the (much larger) Stark shift due to the interaction of the molecular frame dipole moment of HfF$^+$ with the *rotating* electric field. The latter gives rise to the energy splitting between two Stark doublets and does not contribute to $f(\mathcal{B}_{\rm rot},\tilde{\mathcal{D}},\tilde{\mathcal{R}})$.

## III. THEORETICAL METHODS

Following Refs. [13,14], the energy levels and wave functions of the $^{180}$Hf$^{19}$F$^+$ ion are obtained by numerical diagonalization of the molecular Hamiltonian ($\hat{\mathbf{H}}_{\rm mol}$) in external variable electric $\mathbf{E}(t)$ and magnetic $\mathbf{B}(t)$ fields over the basis set of the electronic-rotational wave functions

$$\Psi_\Omega\theta^J_{M,\Omega}(\alpha,\beta)U^I_{M_I}. \qquad (4)$$

Here, $\Psi_\Omega$ is the electronic wave function, $\theta^J_{M,\Omega}(\alpha,\beta)=\sqrt{(2J+1)/4\pi}\,D^J_{M,\Omega}(\alpha,\beta,\gamma=0)$ is the rotational wave function, $\alpha,\beta,\gamma$ are Euler angles, $U^I_{M_I}$ is the nuclear spin wave functions, $M$ ($\Omega$) is the projection of the molecule angular momentum, $\mathbf{J}$, on the laboratory $\hat{z}$ (internuclear $\hat{n}$) axis, and $M_I=\pm1/2$ is the projection of the nuclear angular momentum on the same axis. Note that $M_F=M_I+M$ is not equal to $m_F$. The latter, as stated above, is the projection of the total momentum on the rotating electric field.

We write the molecular Hamiltonian for $^{180}$Hf$^{19}$F$^+$ in the form

$$\hat{\mathbf{H}}_{\rm mol}=\hat{\mathbf{H}}_{\rm el}+\hat{\mathbf{H}}_{\rm rot}+\hat{\mathbf{H}}_{\rm hfs}+\hat{\mathbf{H}}_{\rm ext}. \qquad (5)$$

Here, $\hat{\mathbf{H}}_{\rm el}$ is the electronic Hamiltonian,

$$\hat{\mathbf{H}}_{\rm rot}=B_0\mathbf{J}^2-2B_0(\mathbf{J}\cdot\mathbf{J}^e) \qquad (6)$$

is the Hamiltonian of the rotation of the molecule, and $B_0=0.2989$ cm$^{-1}$ [15] is the rotational constant.

$$\hat{\mathbf{H}}_{\rm hfs}=g_{\rm F}\mu_N\mathbf{I}\cdot\sum_i\left(\frac{\boldsymbol{\alpha}_i\times\boldsymbol{r}_i}{r_i^3}\right) \qquad (7)$$

is the hyperfine interaction between electrons and flourine nuclei, $g_F=5.25773$ is the $^{19}$F nucleus $g$ factor, $\mu_N$ is the nuclear magneton, and

$$\hat{\mathbf{H}}_{\rm ext}(\mathbf{E}_{\rm static},\mathbf{B}_{\rm static},\mathcal{E}_{\rm rot},\mathcal{B}_{\rm rot}) = \mu_B(\mathbf{L}^e-g_S\mathbf{S}^e)\cdot\mathbf{B}(t)-g_{\rm F}\frac{\mu_N}{\mu_B}\mathbf{I}\cdot\mathbf{B}(t)-\mathbf{D}\cdot\mathbf{E}(t) \qquad (8)$$

describes the interaction of the molecule with external variable magnetic and electric fields. Here, $g_S=-2.0023$ is a free-electron $g$ factor, $\mu_{\rm B}$ is the Bohr magneton, $\mathbf{J}^e=\mathbf{L}^e+\mathbf{S}^e$, $\mathbf{L}^e$ and $\mathbf{S}^e$ are the total electronic, electronic orbital, and electronic spin momentum operators, respectively, and $\mathbf{D}$ is the dipole moment operator. The variable field may be expressed in terms of components of a static field and a field that rotates in the $xy$

plane,

$$\mathbf{E}(t) = \mathbf{E}_{\rm static} + \mathbf{E}_{\rm rot}(t), \tag{9}$$

$$\mathbf{E}_{\rm rot}(t) = \mathcal{E}_{\rm rot}[\hat{x}\cos(\omega_{\rm rot}t) + \tilde{\mathcal{R}}\hat{y}\sin(\omega_{\rm rot}t)], \tag{10}$$

$$\mathbf{B}(t) = \mathbf{B}_{\rm static} + \mathbf{B}_{\rm rot}(t), \tag{11}$$

$$\mathbf{B}_{\rm rot}(t) = \mathcal{B}_{\rm rot}[\hat{x}\cos(\omega_{\rm rot}t) + \tilde{\mathcal{R}}\hat{y}\sin(\omega_{\rm rot}t)], \tag{12}$$

where $\tilde{\mathcal{R}} = \pm 1$ defines the direction of rotation along the $\hat{z}$ axis: $\vec{\omega}_{\rm rot} = \tilde{\mathcal{R}}\omega_{\rm rot}\hat{z}$. $\tilde{\mathcal{R}} = +1(-1)$ if the fields rotate counterclockwise (clockwise) around the $\hat{z}$ axis. Below we put $\omega_{\rm rot}/2\pi = 250{,}150$ kHz, $\mathcal{E}_{\rm rot} = 24{,}20$ V/cm, which are the values used in the experiment [3]. Note that $\omega_{\rm rot}$ and $\mathcal{E}_{\rm rot}$ are always positive. In this paper, the time dependence of the external fields is accounted for using two approaches. In the first (or I below) approach, the transition to the rotating frame is performed:

$$\hat{\mathbf{H}}^{\rm I}_{\rm mol} = \hat{\mathbf{H}}_{\rm el} + \hat{\mathbf{H}}_{\rm rot} + \hat{\mathbf{H}}_{\rm hfs} + \hat{\mathbf{H}}_{\rm ext}(\mathbf{E}_{\rm static} + \mathcal{E}_{\rm rot}\hat{x}, \mathbf{B}_{\rm static} + \mathcal{B}_{\rm rot}\hat{x}, \mathcal{E}_{\rm rot} = 0, \mathcal{B}_{\rm rot} = 0) - \vec{\omega}_{\rm rot}\cdot\mathbf{F}. \tag{13}$$

In the second (or II below) approach, the interaction with rotating fields,

$$\begin{aligned}&\left[\mu_{\rm B}(\mathbf{L}^e - g_S\mathbf{S}^e) - g_{\rm F}\frac{\mu_N}{\mu_B}\mathbf{I}\right]\cdot\mathbf{B}_{\rm rot}(t) - \mathbf{D}\cdot\mathbf{E}_{\rm rot}(t)\\ &= (\mathcal{B}_{\rm rot}/2)\left[\mu_{\rm B}\left(L^e_{-\mathcal{R}} - g_S S^e_{-\mathcal{R}}\right) - g_{\rm F}\frac{\mu_N}{\mu_B}I_{-\mathcal{R}}\right]e^{i\omega_{\rm rot}t}\\ &\quad - (\mathcal{E}_{\rm rot}/2)D_{-\mathcal{R}}e^{i\omega_{\rm rot}t} + (\mathcal{B}_{\rm rot}/2)\left[\mu_{\rm B}\left(L^e_{+\mathcal{R}} - g_S S^e_{+\mathcal{R}}\right)\right.\\ &\quad \left. - g_{\rm F}\frac{\mu_N}{\mu_B}I_{+\mathcal{R}}\right]e^{-i\omega_{\rm rot}t} - (\mathcal{E}_{\rm rot}/2)D_{+\mathcal{R}}e^{-i\omega_{\rm rot}t},\end{aligned} \tag{14}$$

is replaced by the interaction with the corresponding quantized electromagnetic fields,

$$\begin{aligned}\hat{\mathbf{H}}_{\rm quant} &= \hbar\omega_{\rm rot}a^+a - \sqrt{\frac{2\pi\hbar\omega_{\rm rot}}{V}}\\ &\quad\times\mathcal{B}_{\rm rot}\left[\mu_{\rm B}\left(L^e_{-\mathcal{R}} - g_S S^e_{-\mathcal{R}}\right) - g_{\rm F}\frac{\mu_N}{\mu_B}I_{-\mathcal{R}}\right]a^+\\ &\quad - \mathcal{E}_{\rm rot}D_{-\mathcal{R}}a^+ + \mathcal{B}_{\rm rot}\left[\mu_{\rm B}\left(L^e_{+\mathcal{R}} - g_S S^e_{+\mathcal{R}}\right)\right.\\ &\quad\left. - g_{\rm F}\frac{\mu_N}{\mu_B}I_{+\mathcal{R}}\right]a - \mathcal{E}_{\rm rot}D_{+\mathcal{R}}a,\end{aligned} \tag{15}$$

where $a^+$ and $a$ are photon creation and annihilation operators, $V$ is the volume of the system,

$$D_\pm = D_x \pm iD_y, \tag{16}$$

and similar notation for the other vectors. To work with Hamiltonian (15), one needs to add the quantum number $|n\rangle$, where $n = \frac{V}{8\hbar\pi\omega_{\rm rot}} \gg 1$ is the number of photons. The approach was developed in Ref. [16]. Then the total Hamiltonian in approach (II) is

$$\hat{\mathbf{H}}^{\rm II}_{\rm mol} = \hat{\mathbf{H}}_{\rm el} + \hat{\mathbf{H}}_{\rm rot} + \hat{\mathbf{H}}_{\rm hfs} + \hat{\mathbf{H}}_{\rm ext}(\mathbf{E}_{\rm static}, \mathbf{B}_{\rm static}, \mathcal{E}_{\rm rot} = 0, \mathcal{B}_{\rm rot} = 0) + \hat{\mathbf{H}}_{\rm quant}. \tag{17}$$

For the current study, we have considered the following low-lying electronic basis states: $^3\Delta_1$, $^3\Delta_2$, $^3\Pi_{0^+}$, and $^3\Pi_{0^-}$. Electronic matrix elements required to evaluate the molecular Hamiltonian have been taken from Ref. [17], with the exception of the hyperfine structure constant $A_\parallel = -62.0$ MHz and dipole moment $D_\parallel = -1.40$ a.u. for $^3\Delta_1$, which have been taken from Ref. [3].

Only the static fields parallel to $\vec{\omega}_{\rm rot}$ ($\hat{z}$ axis) are allowed in the first scheme, whereas the second approach is valid for arbitrary $\mathbf{E}_{\rm static}, \mathbf{B}_{\rm static}$. Including other rotating and oscillating fields with arbitrary directions and frequencies is also possible within approach (II). However, working with the second approach, one should ensure the convergence of the result with the number $N$ of photon states, $|n_0 - N\rangle$, $|n_0 - N + 1\rangle, \ldots, |n_0 - 1\rangle, |n_0\rangle$, $|n_0 + 1\rangle, \ldots, |n_0 + N - 1\rangle$, $|n_0 + N\rangle$, included in the calculation. In the absence of external fields and with the static fields $\mathcal{E}_z\hat{z}$, $\mathcal{B}_z\hat{z}$ (aligned along the $\hat{z}$ axis) with sufficiently large number of photon states, both approaches should give the same result.

## IV. RESULTS AND DISCUSSIONS

In Fig. 1, results for $f(\mathcal{B}_{\rm rot}, \tilde{\mathcal{D}}, \tilde{\mathcal{R}} = +1)$ with $\tilde{\mathcal{D}} = +1$ and $\tilde{\mathcal{D}} = -1$ as functions of $\mathcal{B}_{\rm rot}$ are given, calculated within the two approaches. The calculated values correspond to Zeeman splitting between the $m_F = \pm 3/2$ sublevels for lower ($\tilde{\mathcal{D}} = +1$) and upper ($\tilde{\mathcal{D}} = -1$) Stark doublets. Approach (II) with $N = 3$ is in complete agreement with approach (I). Adding $\mathcal{E}_z\hat{z}$ leads to the tilting of the rotating quantization axis away from the plane of rotation by small angle $\mathcal{E}_z/\mathcal{E}_{\rm rot}$. This changes the accumulated Berry phase and shifts the avoided crossing from the $\mathcal{B}_{\rm rot} = 0$ point. The effect is described in detail in Ref. [9].

The electronic matrix elements used in the present paper to evaluate the molecular Hamiltonian correspond to the negative $g$ factor of $J = 1, F = 3/2$ [17]. One sees from Fig. 1 that Zeeman energy splittings calculated with $\mathcal{E}_z = +0.3$ mV/cm [dotted (blue) and dot-dashed (purple) lines] are smaller than ones calculated with $\mathcal{E}_z = 0$ [solid (red) and dashed (green) lines] for $\mathcal{B}_{\rm rot} > 0.5$ mG. (For infinitely small $\mathcal{E}_z > 0$, the effect will persist for any $\mathcal{B}_{\rm rot} > 0$.) Thus, the data from Fig. 1 mean that for a negative $g$ factor of $J = 1, F = 3/2$, positive $\mathcal{B}_{\rm rot}$, counterclockwise rotation of $\mathbf{E}_{\rm rot}$, and the addition of static electric field $\mathbf{E}_{\rm static} = \mathcal{E}_z\hat{z}, \mathcal{E}_z > 0$ lead to a decrease of Zeeman energy splittings for the $H\,^3\Delta_1$ ($J = 1, F = 3/2, |m_F| = 3/2$) Stark pairs. This result confirms the theory of Ref. [10] used to determine the sign for the $g$ factor of $J = 1, F = 3/2$ from observed Zeeman energy splittings.

The interaction of $e$EDM with the effective electric field $E_{\rm eff} = 22.5$ GV/cm in the molecule,

$$\hat{\mathbf{H}}_{\rm edm} = d_e E_{\rm eff}(\hat{n}\cdot\mathbf{J}), \tag{18}$$

gives rise to the $f^{\mathcal{BD}}$ channel to be measured in the experiment. To reach the maximum value $f^{\mathcal{BD}} = 2d_e E_{\rm eff}$, laboratory electric field $\mathcal{E}_{\rm rot}$ must be large enough to fully polarize

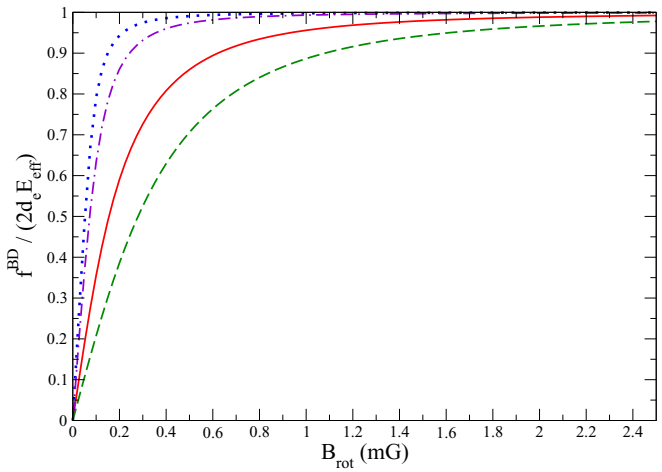


FIG. 2. Calculated $e$EDM-induced $f^{\mathcal{BD}}$ splitting. The solid (red) line corresponds to $\omega_{\rm rot}/2\pi = 250$ kHz, $\mathcal{E}_{\rm rot} = 24$ V/cm; the dashed (green) line corresponds to $\omega_{\rm rot}/2\pi = 250$ kHz, $\mathcal{E}_{\rm rot} = 20$ V/cm; the dotted (blue) line corresponds to $\omega_{\rm rot}/2\pi = 150$ kHz, $\mathcal{E}_{\rm rot} = 24$ V/cm; and the dot-dashed (purple) line corresponds to $\omega_{\rm rot}/2\pi = 150$ kHz, $\mathcal{E}_{\rm rot} = 20$ V/cm.

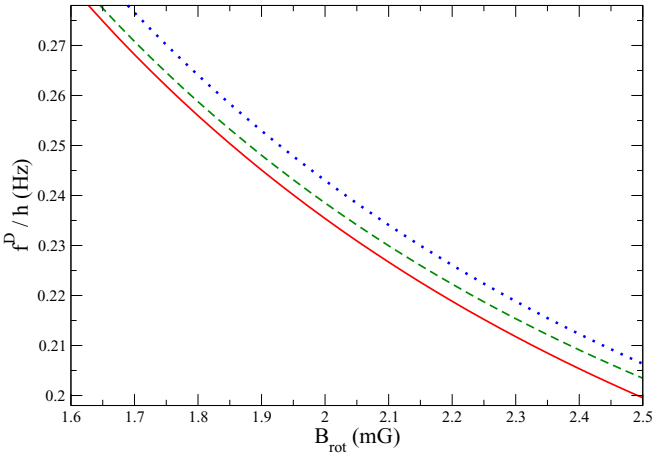


FIG. 3. Calculated $f^{\mathcal{D}}$ as a function of $\mathcal{B}_{\rm rot}$. Solid (red) curve: Interactions with both $^3\Delta_2$ and $^3\Pi_{0^\pm}$ states are taken into account. Dashed (green) curve: Only interactions with the $^3\Pi_{0^\pm}$ states are taken into account. Dotted (blue) curves: Interactions with both $^3\Delta_2$ and $^3\Pi_{0^\pm}$ states are omitted. $\mathcal{E}_{\rm rot} = 24$V/cm, $\omega_{\rm rot}/2\pi = 250$ kHz in the calculations.

the molecule. $J = 1$ $HfF^+$ becomes almost fully polarized for $\mathcal{E}_{\rm rot} > 5$ V/cm [15]. However, the rotation causes the sublevels $m_F = +3/2$ and $m_F = -3/2$ to mix. Therefore, at zero magnetic field, eigenstates are equal-mixed combinations of $m_F = \pm 3/2$ sublevels which have different signs for the $e$EDM shift. Thus the value for magnetic field $\mathcal{B}_{\rm rot}$ also has to be large enough to saturate $f^{\mathcal{BD}}$ at $2d_eE_{\rm eff}$. In Fig. 2, the calculated polarization $P = f^{\mathcal{BD}}/2d_eE_{\rm eff}$ [see Eq. (2)] as a function of $|\mathcal{B}_{\rm rot}|$ is given. Both methods are in agreement. The value for the rotating magnetic field presented in the experiment is given by [3]

$$\mathcal{B}_{\rm rot} = \mathcal{B}'_{\rm axgrad} r_{\rm rot}, \tag{19}$$

where $\mathcal{B}'_{\rm axgrad} = 40$ mG/cm,

$$r_{\rm rot} = \frac{e\mathcal{E}_{\rm rot}}{M\omega^2_{\rm rot}} \tag{20}$$

is the ion's radius of circular motion, and $M = 199$ amu is the mass of $HfF^+$. For $\omega_{\rm rot}/2\pi = 250$ kHz, Eqs. (19) and (20) give $\mathcal{B}_{\rm rot} = 1.87$ and $\mathcal{B}_{\rm rot} = 1.56$ G for $\mathcal{E}_{\rm rot} = 24$ and $\mathcal{E}_{\rm rot} = 20$ V/cm, respectively. Then, according to Fig. 2, $P = 98.5\%$ and $P = 95\%$ efficiency is reached for $\mathcal{E}_{\rm rot} = 24$ and $\mathcal{E}_{\rm rot} = 20$ V/cm, which corresponds to reduced effective electric field $E_{\rm eff} = 22.2$ and $E_{\rm eff} = 21.3$ GV/cm, respectively. Note that $E_{\rm eff}$ cannot be measured, but it is required for extracting the EDM value from the measured $f^{BD}$ [see Eq. (2)].

As mentioned above, one of the main systematic effects in the experiment for $e$EDM search on $^{180}Hf^{19}F^+$ ions comes from doublet population contamination. The desired Stark level doublet is populated using Raman transfer, $^1\Sigma^+ \rightarrow {}^3\Pi_{0^+} \rightarrow {}^3\Delta_1$. The upper and lower Stark doublets are resolved by approximately nine times the Doppler width. Therefore, Raman transfer to an undesired Stark doublet is very unlikely. However, spontaneous decay from excited states can occur to both Stark pairs, resulting in doublet population contamination [3]. The extent of the contamination is estimated from the difference between measured and predicted (calculated) values of $f^{\mathcal{D}}$. In Fig. 3, the calculated $f^{\mathcal{D}}$ as a function of $\mathcal{B}_{\rm rot}$ for $\omega_{\rm rot}/2\pi = 250$ kHz, $\mathcal{E}_{\rm rot} = 24$ V/cm is given. One sees that accounting for interaction with $^3\Delta_2$, $^3\Pi_{0^+}$, and $^3\Pi_{0^-}$ electronic states is important for the accurate calculation of $f^{\mathcal{D}}$ and changes the result by about 4%. In Fig. 4, the calculated $f^{\mathcal{D}}$ as a function of $f^0$ and experimental value [3] $f^0/h = 22.9985(13)$ Hz, $f^{\mathcal{D}}/h = 32.0(1.0)$ mHz for $\omega_{\rm rot}/2\pi = 150$ kHz, $\mathcal{E}_{\rm rot} = 24$ V/cm is given. To plot Fig. 4, both $f^{\mathcal{D}}$ and $f^0$ are assumed to be functions of $\mathcal{B}_{\rm rot}$. One sees that accounting for the contribution of interaction with $^3\Delta_2$, $^3\Pi_{0^+}$, and $^3\Pi_{0^-}$ electronic states leads to agreement between the measured and calculated values.

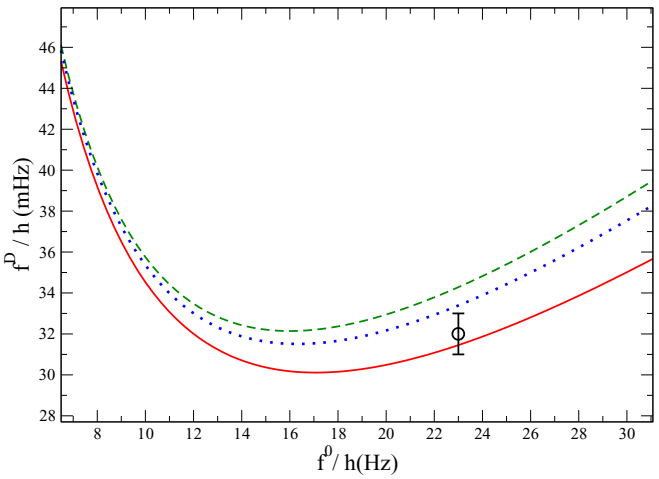


FIG. 4. Calculated $f^{\mathcal{D}}$ as a function of $f^0$. Solid (red) curve: Interactions with both $^3\Delta_2$ and $^3\Pi_{0^\pm}$ states are taken into account. Dashed (green) curve: Only interactions with the $^3\Pi_{0^\pm}$ states are taken into account. Dotted (blue) curves: Interactions with both $^3\Delta_2$ and $^3\Pi_{0^\pm}$ states are omitted. $\mathcal{E}_{\rm rot} = 24$V/cm, $\omega_{\rm rot}/2\pi = 150$ kHz. The circle is the experimental value.

## V. CONCLUSION

We have calculated the effective electric field $E_{\rm eff}$ which takes into account incomplete polarization and energy splittings for $J = 1$, $F = 3/2$, $|m_F| = 3/2$ hyperfine levels of the $^3\Delta_1$ electronic state as functions of the external electric and magnetic fields.

We found that for accurate evaluation of $f^{\mathcal{D}}$ frequency, the interaction with the $^3\Delta_2$, $^3\Pi_{0^+}$, and $^3\Pi_{0^-}$ electronic states has to be taken into account. Calculation of $f^{\mathcal{D}}$ is required for the estimation of systematic effects related to doublet population contamination. For the current experimental result, the statistical uncertainty is about four times larger than the systematic one [see Eq. (1)]. It is clear, however, that for the second-generation of the $e$EDM measurement (which will provide an order-of-magnitude-higher statistical sensitivity), the systematic effects should be evaluated more accurately as well. The agreement between experimental and theoretical values of $f^{\mathcal{D}}$ reached in the present work indicates that systematic effects in the experiment can be reduced significantly, thus confirming the prospects of $HfF^+$ for the electron electric dipole moment search.

## ACKNOWLEDGMENT

The work is supported by the Russian Science Foundation Grant No. 14-31-00022.

[1] E. D. Commins, Adv. At. Mol. Opt. Phys. **40**, 1 (1999).
[2] T. Chupp and M. Ramsey-Musolf, Phys. Rev. C **91**, 035502 (2015).
[3] W. B. Cairncross, D. N. Gresh, M. Grau, K. C. Cossel, T. S. Roussy, Y. Ni, Y. Zhou, J. Ye, and E. A. Cornell, Phys. Rev. Lett. **119**, 153001 (2017).
[4] J. Baron, W. C. Campbell, D. DeMille, J. M. Doyle, G. Gabrielse, Y. V. Gurevich, P. W. Hess, N. R. Hutzler, E. Kirilov, I. Kozyryev *et al.*, Science **343**, 269 (2014).
[5] A. N. Petrov, N. S. Mosyagin, T. A. Isaev, and A. V. Titov, Phys. Rev. A **76**, 030501(R) (2007).
[6] A. N. Petrov, N. S. Mosyagin, and A. V. Titov, Phys. Rev. A **79**, 012505 (2009).
[7] L. V. Skripnikov, J. Chem. Phys. **147**, 021101 (2017).
[8] T. Fleig, Phys. Rev. A **96**, 040502 (2017).
[9] A. Leanhardt, J. Bohn, H. Loh, P. Maletinsky, E. Meyer, L. Sinclair, R. Stutz, and E. Cornell, J. Mol. Spectrosc. **270**, 1 (2011).
[10] H. Loh, K. C. Cossel, M. C. Grau, K.-K. Ni, E. R. Meyer, J. L. Bohn, J. Ye, and E. A. Cornell, Science **342**, 1220 (2013).
[11] J. Baron, W. C. Campbell, D. DeMille, J. M. Doyle, G. Gabrielse, Y. V. Gurevich, P. W. Hess, N. R. Hutzler, E. Kirilov, I. Kozyryev *et al.*, New J. Phys. **19**, 073029 (2017).
[12] A. N. Petrov, Phys. Rev. A **95**, 062501 (2017).
[13] A. N. Petrov, Phys. Rev. A **83**, 024502 (2011).
[14] A. N. Petrov, L. V. Skripnikov, A. V. Titov, N. R. Hutzler, P. W. Hess, B. R. O'Leary, B. Spaun, D. DeMille, G. Gabrielse, and J. M. Doyle, Phys. Rev. A **89**, 062505 (2014).
[15] K. C. Cossel, D. N. Gresh, L. C. Sinclair, T. Coffey, L. V. Skripnikov, A. N. Petrov, N. S. Mosyagin, A. V. Titov, R. W. Field, E. R. Meyer *et al.*, Chem. Phys. Lett. **546**, 1 (2012).
[16] A. N. Petrov, Phys. Rev. A **91**, 062509 (2015).
[17] A. N. Petrov, L. V. Skripnikov, and A. V. Titov, Phys. Rev. A **96**, 022508 (2017).